Bifurcation analysis of stationary and oscillating domains in semiconductor superlattices with doping fluctuations

M. Patra, G. Schwarz, and E. Schöll
Institut für Theoretische Physik, Technische Universität Berlin, Hardenbergstraße 36, 10623 Berlin, Germany
(Received 10 January 1997; revised manuscript received 9 July 1997)

We investigate the effects of frozen-in spatial fluctuations of the doping density on the different forms of spatiotemporal pattern formation found in weakly coupled *n*-doped superlattices as described by a simple microscopic model. For heavy doping, multistable field domains are observed, while for lower doping space-charge oscillations are found. The corresponding bifurcation scenarios are discussed. We demonstrate that there occurs a qualitative change once the degree of disorder exceeds a certain threshold. For the case of moderate disorder and heavy doping, a direct correlation between the peak current of each branch of the current-voltage characteristic and the doping density in the corresponding quantum well is derived and applied to analyze a measured characteristic. [S0163-1829(98)05103-0]

I. INTRODUCTION

The formation of electric field domains in a semiconductor superlattice in the high-field regime was already predicted by Esaki and Chang[1] and verified later for both doped and optically excited superlattices.[2–4] These results were explained using different theoretical models.[5–7] Later, time-dependent features such as transient[8] and persistent current oscillations were also found both in simulations[9,10] and experimentally.[11] Recently, the agreement of simulations with experimental results was considerably improved by taking into account growth-related disorder and structural imperfections.[12–16]

For a structurally perfect superlattice general features of stationary field domains[17] and self-oscillations[18] have recently been analyzed in terms of a simple, analytically tractable model.

The purpose of the present paper is to gain a deeper understanding of the different nonlinear spatiotemporal modes and their sensitivity to the presence of growth-related doping fluctuations. We do this by presenting a comprehensive analysis of bifurcation scenarios not only in dependence on bias voltage and mean donor density but by taking the degree of disorder into account as a third, equally important system parameter. The different regimes of stationary multistable field domains and self-sustained oscillations are investigated in the framework of the microscopic model of Ref. 12.

The superlattices discussed in this paper consist of N (typically 40) GaAs quantum wells of width l separated by $N-1$ AlAs barriers of width b. The values used in the simulation are summarized in Table I. The wells are n doped with an average doping density (per unit volume) N_D. Due to the relatively wide barriers considered, the coupling between different quantum wells is weak, and thus each electron is effectively localized in a quantum well. Charge transport then occurs mainly through sequential tunneling between adjacent wells.

We use the electron concentrations (per unit area) in the kth energy level of the ith quantum well, $n_k^{(i)}$, as the dynamic variables of our system. For moderate applied voltages, we can restrict ourselves to the two lowest energy levels, $k=1,2$. The rate of change of the electron densities can then be expressed as[6]

$$\dot{n}_1^{(i)} = R_1^{(i)} n_1^{(i-1)} - R_1^{(i+1)} n_1^{(i)} - n_1^{(i)} (X_r^{(i+1)} + X_l^{(i)}) + n_2^{(i+1)} Y_l^{(i+1)} + n_2^{(i-1)} Y_r^{(i)} + n_2^{(i)} / \tau_{21}, \tag{1}$$

$$\dot{n}_2^{(i)} = R_2^{(i)} n_2^{(i-1)} - R_2^{(i+1)} n_2^{(i)} - n_2^{(i)} (Y_l^{(i)} + Y_r^{(i+1)}) + n_1^{(i-1)} X_r^{(i)} + n_1^{(i+1)} X_l^{(i+1)} - n_2^{(i)} / \tau_{21}, \tag{2}$$

where τ_{21} is the intersubband relaxation time. $R_k^{(i)}$ is the transition probability per unit time for electrons crossing the ith barrier [located between the ith and the $(i+1)$st well] between equivalent subbands k of two adjacent wells and is modeled by a simple phenomenological approximation.[19] The coefficients $X_r^{(i)}$, $X_l^{(i)}$, $Y_r^{(i)}$, and $Y_l^{(i)}$ for transitions between different subbands of adjacent wells are determined by resonant tunneling and are calculated from quantum mechanical perturbation theory.[6] X stands for transitions from the first to the second subband, and Y stands for the reverse process. The subscripts r and l denote resonant tunneling to the right (towards the anode) and to the left (towards the cathode), respectively. All transport coefficients depend strongly upon the electric field $F^{(i)}$ in the respective barrier.

For a realistic modeling of the measured current-voltage characteristics, spatial fluctuations of the structural parameters, i.e., the widths of the barriers b and the quantum wells

TABLE I. Parameters of the superlattices used in the simulations.

Width of GaAs quantum wells	$b = 90$ Å
Width of AlAs barriers	$l = 15$ Å
Number of quantum wells	$N = 40$
Relative permittivity of GaAs	$\epsilon_W = 13.2$
Intersubband relaxation time	$\tau_{21} = 1$ ps
Lattice temperature	$T_L = 5$ K
Conduction band discontinuity	$V_0 = 982$ meV

l as well as the doping density N_D must be included. Fluctuations of these three quantities have already been examined in Refs. 12 and 14, where it was inferred from a comparison with experiment that doping fluctuations are the most likely form of microscopic disorder responsible for the irregular shapes of measured current-voltage characteristics.

To model doping fluctuations, we introduce local donor densities, $N_D^{(i)}=(1+\alpha e^{(i)})N_D$ in the ith quantum well, which are distributed around a mean value N_D and parameterized by a random sequence of N values $\{e^{(i)}\}$ and a scaling parameter α that quantifies the degree of disorder without changing the individual random sequence. For the computations presented in this paper, we choose $\{e^{(i)}\}$ to be equidistributed in the interval $[-1,1]$ but the concept is easily extended to more general distributions.

The fields are related to the electron densities and the doping densities by the discrete version of Gauss' law,

$$\epsilon(F^{(i+1)}-F^{(i)})=e(n_1^{(i)}+n_2^{(i)}-lN_D^{(i)}), \tag{3}$$

where ϵ is the permittivity of GaAs. The total voltage drop across the superlattice must be equal to the external voltage U applied to the sample:

$$\sum_i (l+b)F^{(i)}=U, \tag{4}$$

which represents a global coupling condition for the electron densities in the system.

The sample contacts are treated as two additional ''virtual'' quantum wells denoted by $i=0$ and $i=N+1$, in which the electron densities are fixed at $n_1^{(i)}=2N_D$ and $n_2^{(i)}=0$. Thus, we use Dirichlet boundary conditions modeling Ohmic contacts as a carrier reservoir created by heavily doped boundary layers. Different boundary conditions, $n_k^{(0)}=n_k^{(1)}$ and $n_k^{(N+1)}=n_k^{(N)}$, which can be conceived as a discrete form of Neumann boundary conditions, have been discussed previously.[6,12,13]

The total current density across the ith barrier, composed of the conduction and the displacement current densities, is given by

$$j=e[n_1^{(i-1)}(R_1^{(i)}+X_r^{(i)})+n_2^{(i-1)}(R_2^{(i)}+Y_r^{(i)})-n_1^{(i)}X_l^{(i)} - n_2^{(i)}Y_l^{(i)}]+\epsilon\dot{F}^{(i)}, \tag{5}$$

and does not depend on the specific quantum well number i.[20]

Let us first discuss the case of a homogeneous stationary field distribution throughout the superlattice (neglecting disorder and boundary effects). By Eq. (3), this is equivalent to the absence of any charge accumulation or depletion, i.e., $n_1^{(i)}+n_2^{(i)}=N_D$. Thus, the electric field is fixed by the applied voltage U, $F^{(i)}=U/[N(l+b)]$, and one can determine the current-voltage characteristic from Eq. (5) taken at the steady state. The macroscopic $j(U)$ characteristic is then related to the local drift velocity $v(F)$ by setting $j(U)=ev(F)N_D$.[15] Both characteristics exhibit two distinct maxima; the first peak is associated with miniband conduction, the second one is caused by resonant tunneling between different energy levels in adjacent wells. Beyond the first peak, there is a regime of negative differential conductivity (NDC).

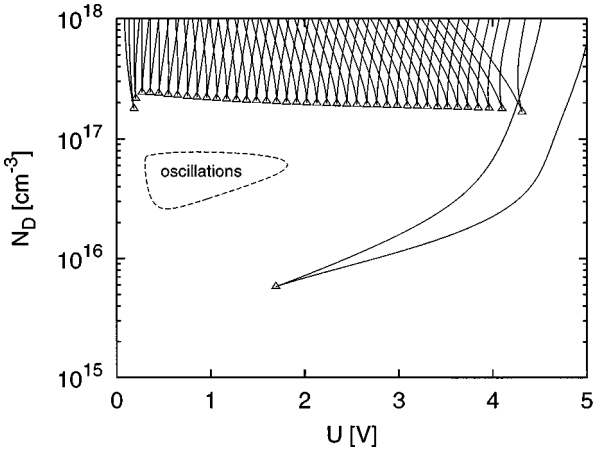

FIG. 1. Phase diagram of spatiotemporal instabilities as a function of external voltage U and doping density N_D for a ''perfect'' superlattice. Saddle-node bifurcations are marked by solid lines, Hopf bifurcations by dashed lines, and cusp points as triangles (△).

II. BIFURCATION SCENARIOS OF SPATIOTEMPORAL PATTERNS

In order to gain insight into the general features of the spatiotemporal scenarios, we shall first briefly review the case of a structurally perfect sample. The different regimes of spatiotemporal behavior found from our simulations are summarized in the phase diagram of Fig. 1. The current-voltage characteristics corresponding to cross sections for different fixed N_D are depicted in Fig. 2.

The spatially homogeneous, N-shaped current-voltage characteristic is stable only at low doping [Fig. 2(a)]. For higher doping, a smeared-out domainlike field distribution forms, and a bistable Z-shaped current-voltage characteristic arises [Fig. 2(b)], indicating a transition between a smeared-out field domain for high current and lower voltage, and an almost homogeneous field distribution for low current and higher voltage. The positions of saddle-node bifurcation points where a stable and an unstable steady-state merge are indicated by diamonds; they form two lines in the lower part of the phase diagram in Fig. 1. At a minimum value of N_D the two lines end in a cusp point where the $j(U)$ characteristic changes from N shaped to Z shaped.

At higher doping, spatiotemporal instabilities lead to self-generated current oscillations associated with the buildup of space charges.[9] Here, the current-voltage characteristic contains a regime of limit cycle oscillations [Fig. 2(c)]. This regime is confined by supercritical Hopf bifurcation points, marked as a closed dashed line in Fig. 1. Note that subcritical Hopf bifurcations can be observed for different boundary conditions.[13]

A typical oscillation is depicted in Fig. 3. The field profile in Fig. 3(a) shows that an inhomogeneous field distribution forms and moves towards the anode. The charge accumulation associated with it [Fig. 3(b)] grows in order to fulfill the global coupling condition (4), and eventually, near the anode, vanishes. Then the whole cycle is repeated.[15] The cor-

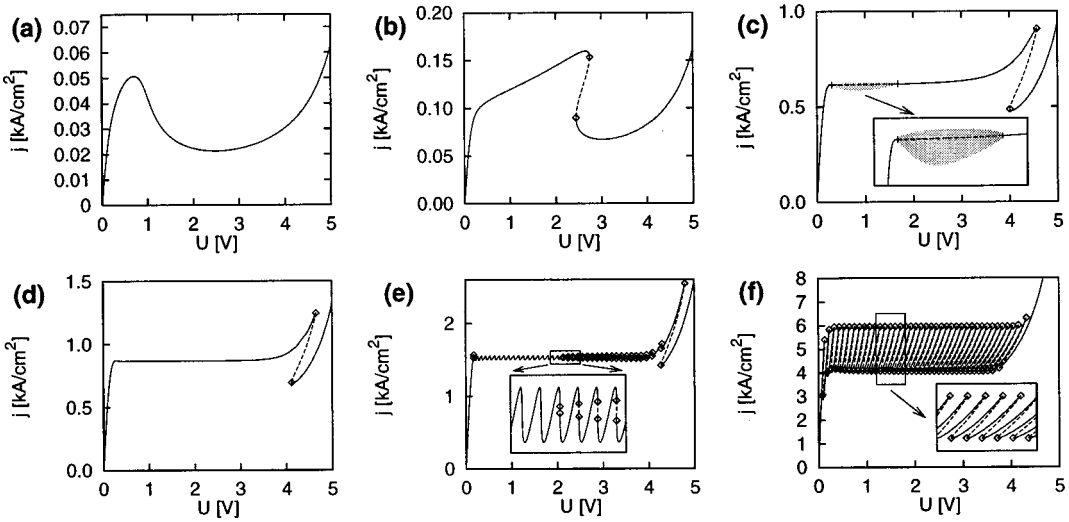

FIG. 2. Current-voltage characteristics for doping densities of (a) $N_D=3.2\times10^{15}$ cm^{-3}, (b) $N_D=10^{16}$ cm^{-3}, (c) $N_D=7\times10^{16}$ cm^{-3}, (d) $N_D=10^{17}$ cm^{-3}, (e) $N_D=2\times10^{17}$ cm^{-3}, (f) $N_D=7.9\times10^{17}$ cm^{-3}. In all current-voltage characteristics presented in this paper, stable stationary states are marked as solid lines, unstable ones as dashed lines, saddle-node bifurcation points as diamonds ($\diamond$) and Hopf bifurcation points as crosses (+). Oscillations are indicated by shaded areas within minimum and maximum current density. The insets show enlarged sections of the respective current-voltage characteristics.

responding oscillation of the current density j is almost perfectly sinusoidal. The oscillation exhibits a square-root dependence of the amplitude upon the distance from the bifurcation point as shown in the inset of Fig. 3(c) for fixed N_D and increasing U. The frequency is not affected by this bifurcation and is determined near the bifurcation point by the imaginary part of the corresponding eigenvalue [Fig. 3(c)]. Similar results are obtained for fixed U and variable N_D. Over the entire oscillatory regime, the frequency varies by approximately 25% similar to what is seen in Ref. 18 for corresponding boundary conditions (cf. the inset of Fig. 13(b) therein). The frequencies calculated there, however, depend strongly on the choice of boundary condition $n^{(0)}=(1+c)N_D$ parametrized by c. The values of c used throughout most of Ref. 18 are very small and thus different from our model, which assumes heavily doped boundary layers. Therefore, most of the results presented in Ref. 18 cannot directly be compared with our results. However, for Neumann boundary conditions we have also found frequencies strongly varying with voltage and decreasing monotonically almost down to zero[21] as in the model of Ref. 18. This is consistent with the results found in Ref. 18, since both types of boundary conditions allow for an (almost) homogeneous field distribution as a stationary solution, in contrast to the heavily doped boundary layer conditions used in the present paper.

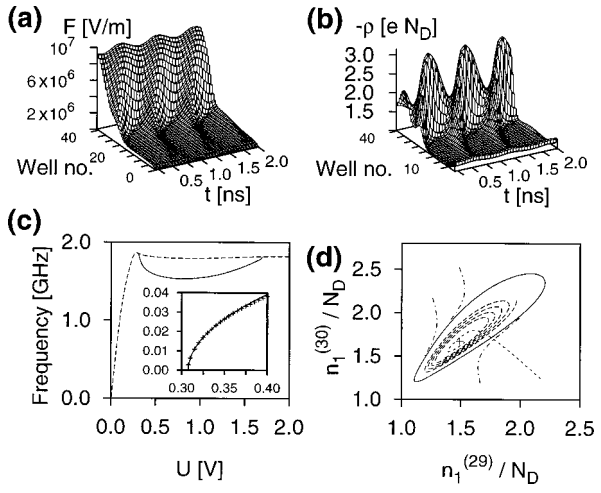

FIG. 3. Limit cycle oscillation ($N_D=5\times10^{16}$ cm^{-3}). (a) Temporal evolution of the field profile F. (b) Temporal evolution of the charge density, ρ ($U=1$ V). (c) Frequency of the oscillation versus U (solid line). The frequency corresponding to the imaginary part of the largest eigenvalue is shown as a dashed line. The inset depicts the amplitude of the current density j (in kA/cm^2) versus U (in V) near one of the Hopf bifurcation points (+). (d) Phase portrait of n_1^{30} vs n_1^{29} (+, unstable fixed point; solid line, limit cycle; dashed line, trajectory lying in the center manifold; dotted line, trajectory starting outside the center manifold; the other trajectories start near the limit cycle).

The dynamics is fast in the directions orthogonal to the center manifold (see, e.g., Ref. 22), in which the limit cycle as well as the corresponding unstable fixed point are embedded [Fig. 3(d)].

Note that in contrast to the formation of stationary field domains, the superlattice must contain a minimum number of quantum wells to enable oscillations.[17] In addition to such charge oscillations of a single domain boundary, at higher doping levels traveling high-field domains embedded between two low-field domains are found if the model is extended to accommodate highly doped boundary layers adjacent to the contacts. Thus current oscillations may also occur at larger doping.

At the highest doping densities, the number of available carriers is sufficient to provide the space charge necessary to form a stable, stationary boundary between a low-field and a high-field domain (cf. Fig. 4). The buildup of a charge accumulation and the subsequent nucleation of field domains is a process of self-organized pattern formation, which is common in semiconductors with negative differential

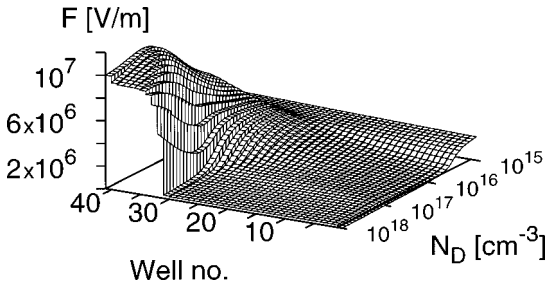

FIG. 4. Field profile as a function of the doping density, N_D, for fixed $U=1$ V.

conductivity.[23–26] However, there are essential differences compared, e.g., to the classical Gunn domain instability, which is associated with a traveling triangular domain. For its existence it is required only that the $v(F)$ characteristic has one rising and one falling branch. In the superlattice, the high- and low-field domains correspond to spatial coexistence of two stable states of the local $j(F)$ characteristic at the same current density,[15] while the Gunn domains have a triangular field profile whose maximum does not attain a second stable state.[24] Different equal area rules have been derived for both cases.[10,15,27,28] If the doping density is sufficiently high, the width of the domain boundary is of the order of the superlattice period. In this case, the domain boundary is localized in a specific quantum well and, in contrast to the Gunn diode, cannot move continuously through the sample but can only jump from one quantum well to the next. As a result, there exist different stable stationary domain states (their number being approximately equal to the number of quantum wells) which arise from different locations of the boundary.

As the domain boundary is shifted from the anode to the cathode with increasing voltage, the current-voltage characteristic exhibits small modulations in the form of sequences of N- [Fig. 2(e)] or Z-shaped [Fig. 2(f)] branches corresponding to different locations of the domain boundary as shown experimentally.[29] The different stable branches are connected by unstable parts as depicted in the insets. Thus the current-voltage characteristic consists of a single continuously connected curve, along which stable and unstable parts alternate. The changes of stability are caused by saddle-node bifurcations, which show up as a complex pattern of intersecting lines in the upper part of Fig. 1. This diagram allows one to determine the positions of the individual current branches as well as, for given parameters U and N_D, the number of multistable states. The two lines of saddle-node bifurcation points belonging to a particular unstable branch merge in a cusp point. Thus, the associated value of N_D is the minimum doping density necessary for multistability and hysteresis of current branches. Since the cusp points lie at slightly different values of N_D, in the respective range of N_D values hysteresis may set on only above a certain threshold voltage as can be seen in the inset of Fig. 2(e). The overall behavior shown in Fig. 2 for the structurally perfect model is similar to the one found in simple phenomenological models.[17,29]

III. EFFECTS OF DOPING FLUCTUATIONS ON FIELD DOMAINS

In the next two sections we will discuss how doping fluctuations affect the spatiotemporal patterns, i.e., the formation of multistable field domains and limit cycle oscillations. First, we focus on field domains.

Figure 5 shows how the current-voltage characteristic changes in the regime of domain formation if the donor density in a single quantum well is either increased (b) or decreased (c) with respect to the unperturbed case (a). It is evident that there exists a direct correlation between the local doping density in the kth well and the peak current of the $(k+1)$th branch of the current-voltage characteristic (counting from the right) corresponding to the location of the domain boundary at the $(k+1)$th well. One can even infer quantitative information about the local doping density from the peak currents, i.e., the positions of the saddle-node bifurcations which mark the end of a stable branch. It is shown analytically in the Appendix under some simplifying assumptions that the maximum current reached on a particular stable branch is proportional to the doping density in the quantum well next to the well at which the domain boundary is located. This opens up the possibility to determine the local values of the ratio $N_D^{(i)}/N_D$ with good precision from measured current-voltage characteristics and thereby characterize the quality of a sample. This procedure has been tested by applying it to numerically simulated characteristics with random doping fluctuations.[30]

It has also been successfully applied to several measured characteristics where it yields reasonable estimates of the degree of disorder. The computed values of the relative variation $\delta_i=(N_D^{(i)}-N_D)/N_D$ of the local doping density in the ith quantum well from the mean doping density N_D are shown in Table II. Thus, the current-voltage characteristic serves as a direct ''fingerprint'' of the microscopic realization of doping fluctuations. For quantum wells close to the

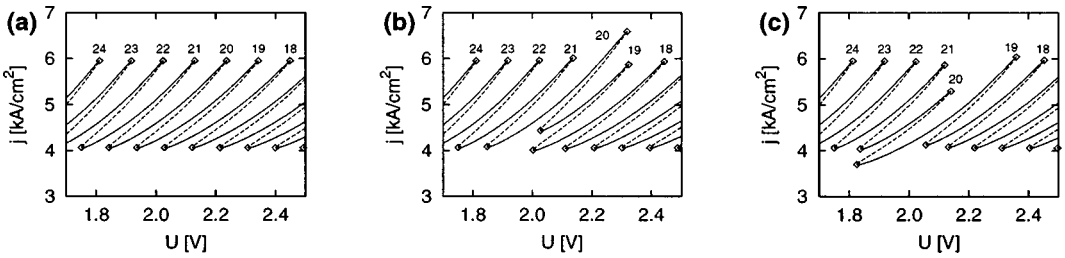

FIG. 5. Part of the current-voltage characteristics in the regime of domain formation ($N_D=7.9\times10^{17}$ cm^{-3}). The doping density in the 20th well is (b) increased by 10%, (c) decreased by 10%. The unperturbed characteristic is displayed in (a). The branches are numbered according to the location of the domain boundary at the kth well.

TABLE II. Computed relative variations $\delta_i=(N_D^{(i)}-N_D)/N_D$ of the doping density in the ith quantum well for the sample investigated in Ref. 29.

$\delta_2=$ 7.5%	$\delta_3=-5.9\%$	$\delta_4=$ 6.2%	$\delta_5=-5.9\%$
$\delta_6=-1.0\%$	$\delta_7=$ 1.0%	$\delta_8=$ 9.3%	$\delta_9=$ 2.7%
$\delta_{10}=$ 7.1%	$\delta_{11}=$ 12.0%	$\delta_{12}=$ 14.0%	$\delta_{13}=$ 3.0%
$\delta_{14}=$ 2.8%	$\delta_{15}=$ 1.4%	$\delta_{16}=-6.6\%$	$\delta_{17}=-14.6\%$
$\delta_{18}=-7.0\%$	$\delta_{19}=-6.9\%$	$\delta_{20}=-8.3\%$	$\delta_{21}=-1.9\%$
$\delta_{22}=-2.1\%$	$\delta_{23}=-4.9\%$	$\delta_{24}=-6.1\%$	$\delta_{25}=-5.2\%$
$\delta_{26}=-1.4\%$	$\delta_{27}=-4.6\%$	$\delta_{28}=$ 0.1%	$\delta_{29}=-2.3\%$
$\delta_{30}=-1.2\%$	$\delta_{31}=$ 3.4%	$\delta_{32}=$ 1.7%	$\delta_{33}=$ 13.8%

cathode or anode, boundary effects become important, and therefore the respective quantum wells have not been included in the analysis. The standard deviation $\sqrt{\Sigma_i \delta_i^2/N}$ of the doping density is 6.7% (corresponding to a value of $\alpha=10.8\%$), which is in good agreement with what is generally known about the properties of the growth process.

Even though the full continuously connected current-voltage characteristic, consisting of alternating stable and unstable branches, shows only slight changes if moderate disorder is introduced, the characteristic that is found under voltage sweep up or sweep down may change qualitatively. Individual branches are shifted and their lengths are changed according to the doping densities in the corresponding quantum wells; thus, some stable branches might be missed out completely during voltage sweep up or sweep down if the doping densities in two adjacent quantum wells differ sufficiently. This is demonstrated in Fig. 6 by comparing voltage sweep up and sweep down (a) with the full stable branches (b). For a given degree of disorder α, the effect of missed-out branches is most pronounced at large doping or high voltage. A careful inspection of the saddle-node lines in the associated phase diagram [Fig. 6(c)] already allows one to determine which branches are missed out for given N_D.

Apart from the single continuously connected current-voltage characteristic, there exist numerous other stationary states, i.e., fixed points of the dynamic system (1), (2), most of them being unstable. Some of them are depicted in Fig. 7(a) for a superlattice without doping fluctuations. With the exception of an additional peak, their field profiles are similar to those of states on the ''standard'' current-voltage characteristic. Almost all such states form ''isolas'' (closed curves) in the $j(U)$ diagram.

We will now focus on a particular class of isolas; a typical member is depicted in Figs. 7(b) (thin dashed line) and 7(c). The field profile displays an additional, smaller peak in the low-field domain. All parts of these isolas are unstable for the doping density considered here but stable branches exist for higher doping. The isolas become more complex when doping fluctuations are introduced since additional branches emerge at cusp points; some of these branches are stable for sufficient degrees of disorder.

If the degree of disorder α is high enough, some isolas merge with the ''standard,'' continuous current-voltage characteristic resulting in a more complex but still continuously connected curve. Figure 8 depicts the same section of the full continuous current-voltage characteristic below (inset) and above (main figure) this threshold. This qualitative change, marking the transition between moderate and strong disorder, is caused by a perturbed transcritical bifurcation (see, e.g., Ref. 31) as schematically sketched in Fig. 9. For low α (left) the unstable isola and the ''standard'' characteristic (stable and unstable branch) are separate. At the threshold value of α (center) the isola and the stable branch join at a transcritical bifurcation point (marked as a square) where two branches exchange their stability. For larger values of α the transcritical bifurcation point splits into two saddle-node points, thereby forming a single connected characteristic into which the isola has been ''inserted.''

If α is increased even further, additional isolas are inserted into the continuous characteristic; some isolas separate off again for even stronger disorder. Furthermore, several isolas may combine to form a single, more complex isola in a similar scenario before merging with the continuously connected current-voltage characteristic, which can thus incorporate a large number of additional branches in a single bifurcation.

IV. EFFECTS OF DOPING FLUCTUATIONS ON OSCILLATIONS

The main effect of disorder in the regime of limit-cycle oscillations is to shift and deform its location in parameter space. For moderate disorder, it is determined by the location of the Hopf bifurcation points [Fig. 6(c), dashed] as in the perfect superlattice (Fig. 1). The change of the oscillation amplitude and frequency for fixed voltage and fixed donor density is only slight.

The effects of an increase (decrease) of the doping density

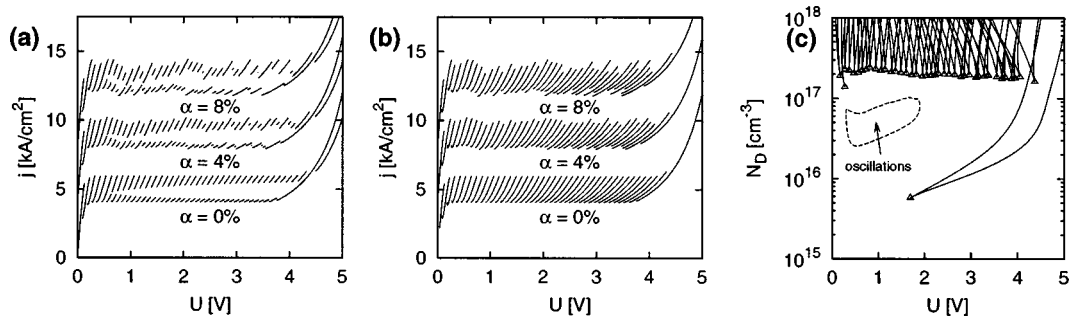

FIG. 6. Current-voltage characteristics for superlattices with different degrees of doping fluctuations α. (a) Characteristics for voltage sweep-up and sweep-down. (b) Stable parts of the full connected current-voltage characteristics ($N_D=7.9\times10^{17}$ cm^{-3}; the vertical scale is shifted for each curve). (c) Phase diagram of mean donor density N_D vs voltage U for $\alpha=8\%$.

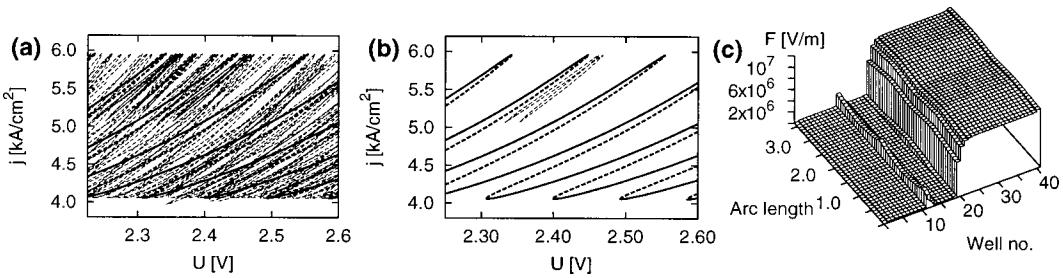

FIG. 7. (a) Current-voltage characteristic including all stable and unstable stationary states. The ''standard'' current-voltage characteristic (bold) contains just a small fraction of all stationary states. (b) The thin dashed line denotes an isola consisting of unstable states only. The ''standard'' current-voltage characteristic is also depicted and marked with bold lines. (c) Field profile for successive points on the isola in (b) parameterized by the arc length of the $j(U)$ diagram ($N_D = 7.9\times10^{17}$ cm^{-3}).

in a single quantum well are depicted in Fig. 10(a) [Fig. 10(b)]. Different curves are marked by the index of the affected quantum well. The influence of a particular quantum well is largest if it is located somewhere in the middle of the superlattice (in the particular superlattice considered here, numerical computations yield the 17th well).

Unfortunately, the total effect of a sequence of random fluctuations [Fig. 10(c)] cannot be predicted from a superposition of the effects of the individual single perturbations as in the regime of multistable field domains. In contrast to the latter case, where the charge accumulation forming the domain boundary is largely confined to a single quantum well, oscillations involve changes of the charges in a large number of quantum wells resulting in a nonlinear interaction. Furthermore, Fig. 10(c) demonstrates that the shape of the regime of oscillations looks very different for different realizations e_i for the same α (here $\alpha = 12\%$) and thus gives no reliable indication of the global degree of disorder. The regime of oscillations tends, however, to become larger with increasing disorder for most of the realizations tested.

For strong disorder, the regime of oscillations may thus extend to doping densities high enough for multistable field domains to form, associated with saddle-node bifurcation. If a Hopf bifurcation and a saddle-node bifurcation coincide this is called a Takens-Bogdanov point (see, e.g., Ref. 32). In a superlattice with strong doping fluctuations, two Takens-Bogdanov points and one cusp point are generated in a single codimension-three bifurcation by appropriately adjusting three control parameters: N_D, U, α. The two Takens-Bogdanov points are connected by a curve of Hopf bifurcation points; if α is increased slightly, this curve merges with the closed curve of Hopf bifurcations found also in superlattices with no or moderate disorder [Fig. 6(c)]. In the phase diagram of the mean doping N_D versus voltage U for fixed α [Fig. 11(a)] this gives a single open curve (dashed), which encloses the shaded area of limit cycle oscillations. Two pairs of full lines corresponding to saddle-node bifurcations of domain states are also shown; each ending in a cusp point (triangle). The inset shows the phase diagram near a Takens-Bogdanov point in more detail.

Since we are discussing a codimension-three bifurcation scenario, it is not sufficient to merely consider the location of the bifurcation points as a function of two parameters. Therefore, the same Takens-Bogdanov points (crosses) are also depicted in the (α, U) plane for fixed N_D in Fig. 11(b). One of the cusp points from (a) is not shown in (b) since it does not depend on the degree of disorder; consequently, there are two saddle-node bifurcation lines extending down to $\alpha = 0$. It can be seen that the Hopf bifurcation line (dashed) connecting the two Takens-Bogdanov points exists only above a minimum value of α.

Details of the current-voltage characteristics corresponding to cross sections of Fig. 11(b) at different α are shown in Fig. 12. For $\alpha = 14.6\%$ (a) no oscillations exist. With increasing α, at first the regime of oscillations (shaded) is limited by two Hopf bifurcation points [Fig. 12(b)]. When the value of the control parameter α is slightly increased, a Hopf bifurcation and a saddle-node bifurcation merge in the first Takens-Bogdanov point. At higher α (c,d) the regime of os-

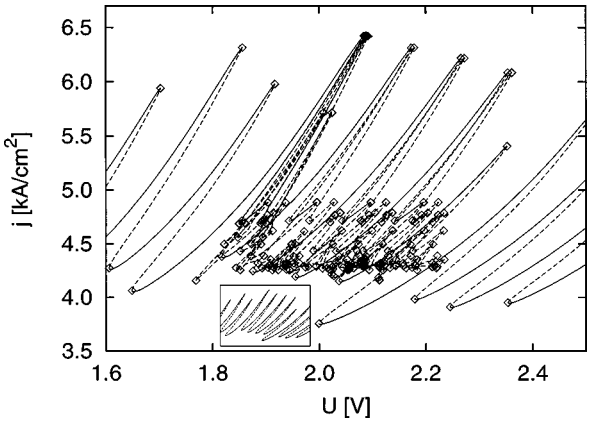

FIG. 8. Current-voltage characteristic for strong disorder ($\alpha = 10\%$). The additional unstable branches are connected to the ''standard'' characteristic at the upper end of the fourth stable branch (starting from the left). The inset depicts the same part of the characteristic for $\alpha = 9\%$ ($N_D = 7.9\times10^{17}$ cm^{-3}).

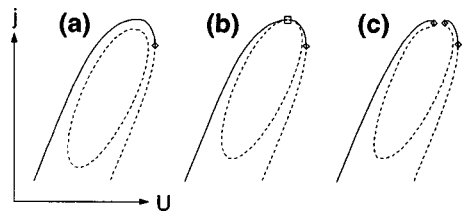

FIG. 9. Schematic current-voltage characteristics illustrating the transition from an isola of unstable states (left) via a transcritical bifurcation (center) to a single continuously connected characteristic (right). The transcritical bifurcation is marked by a square, saddle-node bifurcations are marked by diamonds.

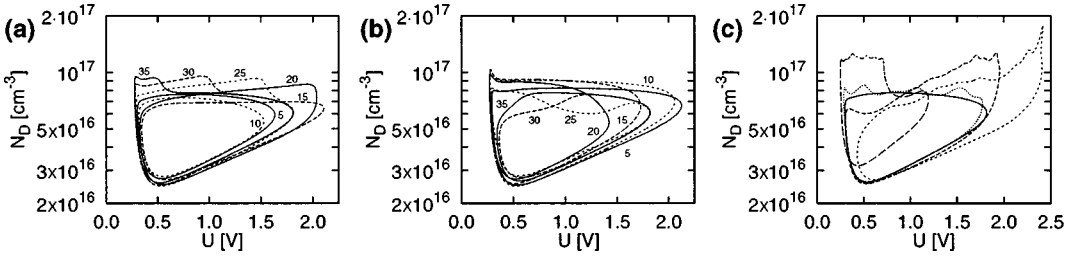

FIG. 10. Phase diagram of the oscillatory regime enclosed by Hopf bifurcation points for superlattices with doping fluctuations. The doping density in a single quantum well is (a) increased, (b) decreased by 12%. Each line is labeled by the number of the quantum well whose doping density is altered. (c) Different realizations of doping disorder $\{e^{(i)}\}$ with $\alpha=12\%$ (solid line: $\alpha=0\%$). The curve with the longest dashes corresponds to the realization used throughout this paper.

cillations is limited at lower U by a Hopf bifurcation, while at higher U it ceases due to a global bifurcation: a homoclinic bifurcation in which a saddle point collides with a limit cycle, forming a saddle loop and subsequently disappearing in the ''blue sky'' (see, e.g., Ref. 22). Here the amplitude of the limit cycle remains finite whereas the frequency tends to zero.[32]

For higher α, we find different bifurcation scenarios. First, the regime of oscillations is no longer bounded from above by a homoclinic (saddle-loop) bifurcation but rather by a saddle-node bifurcation on a limit cycle (see, e.g., Fig. 11(b) for $\alpha\geqslant 15.4\%$), which is another global bifurcation characterized by zero frequency and finite amplitude.[22] For even higher α, a saddle-node bifurcation line originating from the cusp point (triangle) crosses the branch of Hopf bifurcation points [see inset of Fig. 11(b)]. The main regime of oscillations is now limited by two saddle-node bifurcations on the limit cycle (Fig. 13); in addition, there is a small oscillatory regime (left inset) starting at the Hopf bifurcation and being destroyed in a nearby saddle-loop bifurcation. Note that if the temporally averaged current is monitored, as is usually done in experiments, the current-voltage characteristic is expected to exhibit sharp transitions when different stationary and oscillatory regimes are entered.

The saddle-loop bifurcation and the saddle-node bifurcation on a limit cycle result in a sharp decrease of the oscillation frequency down to zero when the voltage approaches one of the bifurcation points (see inset of Fig. 13). Therefore, if a superlattice is operated near one of these bifurcation points, the frequency of the oscillation can be controlled by just changing the applied external voltage U slightly. In Ref. 18, another explanation is given for the increase of the frequency with bias by discussing the space available for the charge monopole to travel. This explanation is not applicable to our model for superlattices of the short length chosen here but becomes relevant only for $N\geqslant 200$ superlattice periods. Voltage tuning of limit cycle oscillations has indeed been observed experimentally in doped superlattices.[18] Such behavior as well as the experimentally found discontinuous switching between different oscillatory modes[33] can be consistently explained also within our model.

V. CONCLUSIONS

In this paper we have theoretically examined two different forms of spatiotemporal pattern formation found in semiconductor superlattices, i.e., stationary multistable field domains and limit cycle oscillations. In superlattices without doping fluctuations as well as in superlattices with moderate disorder, the corresponding regimes are well separated in the parameter space. This reflects the fact that Hopf bifurcations and saddle-node bifurcations are distinguished by different local bifurcation conditions that cannot be simultaneously satisfied. Only for sufficiently strong doping disorder, modeled by spatial fluctuations in the growth direction, do the two regimes of spatiotemporal modes overlap. As a result we

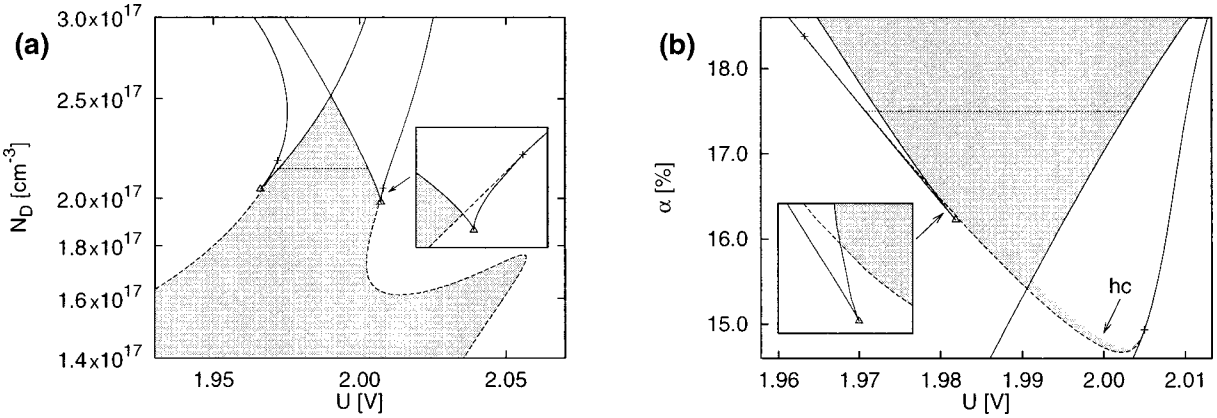

FIG. 11. Part of the phase diagram near the two Takens-Bogdanov points (marked as crosses, +) in a superlattice with strong disorder. The regime of oscillations is shaded. Hopf bifurcations are denoted by dashed lines, saddle-node bifurcations by full lines, and homoclinic bifurcations by the label ''hc.'' The triangles denote cusp points. (a) N_D vs U for fixed $\alpha=17.5\%$. (b) α vs U for fixed $N_D=2.14\times10^{17}$ cm^{-3}. The dotted, horizontal line marks the intersection of the slices of parameter space presented in the two figures.

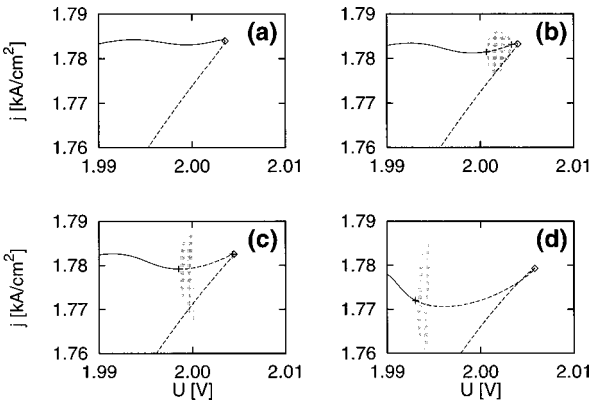

FIG. 12. Details of the current-voltage characteristics for fixed $N_D = 2.14 \times 10^{17}$ cm^{-3} and different degrees of doping disorder. (a) $\alpha = 14.6\%$, (b) $\alpha = 14.7\%$, (c) $\alpha = 14.8\%$, (d) $\alpha = 15.2\%$. Oscillations are shaded.

find complex bifurcation scenarios, including codimension-two and codimension-three points, coexistence and switching between stationary field domain states and different oscillation modes, and global bifurcations that lead to a strong bias tunability of the oscillation frequency.

As far as a quantitative description of the effects of disorder is concerned, the regime of multistable field domains, and thus the case of heavy doping, is the easiest to deal with. The superlattice is divided into a high-field and a low-field domain, and the domain boundary, formed by almost the entire charge accumulation, is localized in a single quantum well. The current through the superlattice is then dominated by the properties of a single quantum well (and a single barrier). Analyzing the peak currents of the different branches of a current-voltage characteristic thus gives quantitative insight into the local doping of the individual wells and hence into the quality of the sample.

ACKNOWLEDGMENTS

We are indebted to F. Prengel and A. Wacker for stimulating discussions, and to W. Jansen for supplying the program Candys/QA. Part of this work was supported by DFG in the framework of Sfb 296.

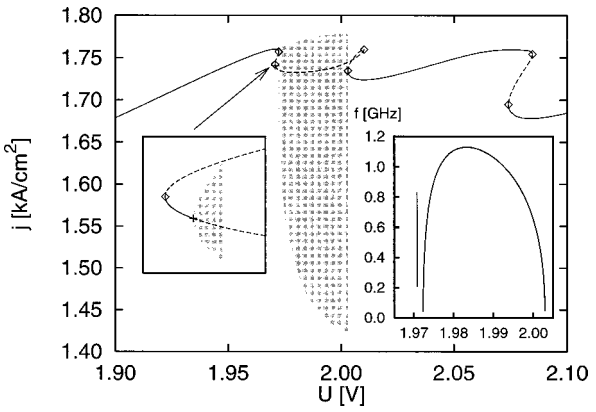

FIG. 13. Current-voltage characteristic corresponding to the dotted line in Fig. 11 ($N_D = 2.14 \times 10^{17}$ cm^{-3}, $\alpha = 17.5\%$). The main regime of limit cycle oscillations (shaded) is bounded on both sides by saddle-node bifurcations on the limit cycle. The left inset shows the region near the Hopf bifurcation (+) in an enlarged scale. The small oscillatory regime (shaded) is bounded on the right-hand side by a saddle-loop bifurcation. The right inset depicts the variation of the frequency f with voltage U.

APPENDIX: CURRENT-VOLTAGE CHARACTERISTIC FOR HEAVILY DOPED SUPERLATTICES

In this appendix, a correlation between the local doping density in the kth quantum well and the current-voltage characteristic in the regime of field domains will be derived analytically under simplifying assumptions. The results are valid irrespectively of the particular transport model used as long as only stationary states are of interest.[21] In the following, we shall assume that the electrons relax fast to the lowest subband in each quantum well, and there is no Fermi degeneracy. The transport equations can then always be written in the form

$$\dot{n}^{(i)} = \sum_j f_{ij} n^{(j)}, \quad i = 1,\ldots, \tag{A1}$$

where $n^{(i)}$ is the electron density in the ith well; f_{ij} denotes the transport coefficient for transitions from the jth to the ith well, and $f_{ii} = -\Sigma_{j \neq i} f_{ji}$ summarizes all transitions out of the ith well. The coefficients are assumed to exhibit a two-peak structure as a function of the electric field $F^{(k)}$ for appropriate values of k.

The coupling between the electron densities $n^{(i)}$, the doping concentrations $N_D^{(i)}$ and the electric fields $F^{(i)}$ is given by Gauss' law (3). An increase in the electron density in a particular quantum well has the same effect upon the electric field, and thus the transport coefficients f_{ij}, as a decrease in the doping density in that well:

$$\frac{\partial f_{ij}}{\partial n^{(k)}} = -\frac{\partial f_{ij}}{\partial N_D^{(k)}}. \tag{A2}$$

As we are only interested in stationary states, we have $\dot{n}^{(i)} = 0 \quad \forall i = 1,\ldots$. Taking the total differential yields

$$0 = \mathrm{d}\dot{n}^{(i)} = \sum_k \frac{\partial \dot{n}^{(i)}}{\partial n^{(k)}} \mathrm{d}n^{(k)} + \sum_k \frac{\partial \dot{n}^{(i)}}{\partial N_D^{(k)}} \mathrm{d}N_D^{(k)}, \quad \forall i. \tag{A3}$$

Applying Eqs. (A1) and (A2), we find

$$0 = \sum_{k,j} \frac{\partial f_{ij}}{\partial n^{(k)}} n^{(j)} (\mathrm{d}n^{(k)} - \mathrm{d}N_D^{(k)}) + \sum_k f_{ik} \mathrm{d}n^{(k)}, \quad \forall i. \tag{A4}$$

Since the coefficients f_{ij} are very sensitive to changes in the electric field and thus to changes in the electron densities, the first term is usually much larger than the second one, which can therefore be neglected. Assuming the matrix $\partial f_{ij} / \partial n^{(k)}$ to be regular, i.e., excluding bifurcation points, this yields the condition

$$\mathrm{d}n^{(k)} = \mathrm{d}N_D^{(k)}, \quad \forall k = 1,\ldots . \tag{A5}$$

Integrating this equation yields

$$n^{(k)} - N_D^{(k)} = \text{const}, \quad \forall k = 1,\ldots . \tag{A6}$$

Thus, the electron densities $n^{(k)}$ adjust to changes in the doping densities $N_D^{(k)}$ in such a way that the electric field distribution $F^{(k)}$ and, consequently, the transport coefficients f_{ij}, do not change. Furthermore, there is a strict one-to-one correspondence between the perturbed and the unperturbed current-voltage characteristic except for very close to a bifurcation point, which is in agreement with the results obtained numerically.

Next, we consider the upper saddle-node bifurcation point of the stable branch for which the domain boundary is located in the ith quantum well. For simplicity we assume that the electrons in each well may only transfer into the adjacent well in the direction of the field, which effectively reduces our model to the one used by Bonilla and co-workers.[7,10] In this case, $f_{i+1,i}=-f_{ii}$, $i=1,\ldots,$ are the only nonzero coefficients, and $f_{i+1,i}=v(F^{(i+1)})$ is the velocity-field characteristic depending only on $F^{(i+1)}$.[15] This saddle-node bifurcation point is determined by the condition that $F^{(i)}$ has moved sufficiently far into the negative differential conductivity (NDC) regime of $f_{i,i-1}$.[10,17]

For all stationary states, the current density

$$j=f_{k+1,k}n^{(k)} \tag{A7}$$

must be independent of k. Let us discuss what the limiting effect in obtaining a higher current density at the bifurcation point is. If we assume the electron densities to be fixed, a stronger current is equivalent to larger values of $f_{k+1,k}$. Since for sufficiently heavy doping all fields $F^{(k)}$ are in the positive differential conductivity regime of $f_{k,k-1}$ except for $k=i$,[17] this is possible by increasing $F^{(k)}$, $k=1,\ldots,$ $k\neq i$, slightly. An overall increase in the electric field means that the applied external voltage has to be increased. The necessary adjustments of the individual electron densities according to Gauss' law are very small as the required increase in $F^{(k)}$ will be approximately the same for all k; the assumption of fixed electron densities is thus satisfied.

Only the current through the ith barrier cannot be increased in this way as $F^{(i)}$ lies in the NDC regime thus making this barrier the limiting element. Since the $(i-1)$th well does not form the domain boundary, $n^{(i-1)}\approx N_D^{(i-1)}$ and, therefore: *The current reached in the upper bifurcation point of a stable branch is proportional to the doping density in the quantum well next to the well (on the cathode side) at which the domain boundary is located.* For a sufficiently high doping density, the upper bifurcation point lies very close to the point of maximum current; thus, for practical purposes it is not necessary to distinguish between these two.

The main source of error in this approximate argument is due to the neglect of the second term in Eq. (A4). If it is included, some electrons are shifted from quantum wells with increased doping into the neighboring wells, mainly in the direction of field.

[1] L. Esaki and L. L. Chang, Phys. Rev. Lett. **33**, 495 (1974).

[2] K. K. Choi, B. F. Levine, R. J. Malik, J. Walker, and C. G. Bethea, Phys. Rev. B **35**, 4172 (1987).

[3] H. T. Grahn, R. J. Haug, W. Müller, and K. Ploog, Phys. Rev. Lett. **67**, 1618 (1991).

[4] *Semiconductor Superlattices, Growth and Electronic Properties*, edited by H. T. Grahn (World Scientific, Singapore, 1995).

[5] B. Laikhtman and D. Miller, Phys. Rev. B **48**, 5395 (1993).

[6] F. Prengel, A. Wacker, and E. Schöll, Phys. Rev. B **50**, 1705 (1994); **52**, 11 518 (1995).

[7] L. L. Bonilla, J. Galán, J. A. Cuesta, F. C. Martínez, and J. M. Molera, Phys. Rev. B **50**, 8644 (1994).

[8] R. Merlin, S. H. Kwok, T. B. Norris, H. T. Grahn, K. Ploog, L. L. Bonilla, J. Galán, J. A. Cuesta, F. C. Martínez, and J. M. Molera, in *Proceedings of the 22nd International Conference on the Physics of Semiconductors, Vancouver 1994*, edited by D. J. Lockwood (World Scientific, Singapore, 1995), p. 1039.

[9] A. Wacker, F. Prengel, and E. Schöll, in *Proceedings of the 22nd International Conference on the Physics of Semiconductors, Vancouver 1994*, edited by D. J. Lockwood (World Scientific, Singapore, 1995), Vol. 2, p. 1075.

[10] L. L. Bonilla, in *Nonlinear Dynamics and Pattern Formation in Semiconductors*, edited by F. J. Niedernostheide (Springer, Berlin, 1995), Chap. 1, pp. 1–20.

[11] J. Kastrup, R. Klann, H. T. Grahn, K. Ploog, L. L. Bonilla, J. Galán, M. Kindelan, M. Moscoso, and R. Merlin, Phys. Rev. B **52**, 13 761 (1995).

[12] A. Wacker, G. Schwarz, F. Prengel, E. Schöll, J. Kastrup, and H. T. Grahn, Phys. Rev. B **52**, 13 788 (1995).

[13] E. Schöll, G. Schwarz, M. Patra, F. Prengel, and A. Wacker, in *Proceedings of the 9th International Conference on Hot Carriers in Semiconductors, Chicago 1995*, edited by K. Hess, J. P. Leburton, and U. Ravaioli (Plenum Press, New York, 1996), pp. 177–181.

[14] G. Schwarz, A. Wacker, F. Prengel, E. Schöll, J. Kastrup, H. T. Grahn, and K. Ploog, Semicond. Sci. Technol. **11**, 475 (1996).

[15] G. Schwarz and E. Schöll, Phys. Status Solidi B **194**, 351 (1996).

[16] G. Schwarz, F. Prengel, E. Schöll, J. Kastrup, H. T. Grahn, and R. Hey, Appl. Phys. Lett. **69**, 626 (1996).

[17] A. Wacker, M. Moscoso, M. Kindelan, and L. L. Bonilla, Phys. Rev. B **55**, 2466 (1997).

[18] J. Kastrup, R. Hey, K. H. Ploog, H. T. Grahn, L. L. Bonilla, M. Kindelan, M. Moscoso, A. Wacker, and J. Galán, Phys. Rev. B **55**, 2476 (1997).

[19] A. A. Ignatov, E. P. Dodin, and V. I. Shashkin, Mod. Phys. Lett. B **5**, 1087 (1991).

[20] E. Schöll and A. Wacker, in *Nonlinear Dynamics and Pattern Formation in Semiconductors and Devices*, edited by F. J. Niedernostheide (Springer, Berlin, 1995), pp. 21–45.

[21] M. Patra, Master's thesis, Technische Universität Berlin, 1996.

[22] J. M. T. Thompson and H. B. Stewart, *Nonlinear Dynamics and Chaos: Geometrical Methods for Engineers and Scientists* (Wiley, Chichester, 1986).

[23] E. Schöll, *Nonequilibrium Phase Transitions in Semiconductors* (Springer, Berlin, 1987).

[24] M. P. Shaw, V. V. Mitin, E. Schöll, and H. L. Grubin, *The Physics of Instabilities in Solid State Electron Devices* (Plenum

Press, New York, 1992).
[25] R. Döttling and E. Schöll, Physica D **67**, 418 (1993).
[26] *Nonlinear Dynamics and Pattern Formation in Semiconductors and Devices*, edited by F. J. Niedernostheide (Springer, Berlin, 1995).
[27] P. N. Butcher, Phys. Lett. **19**, 546 (1965).
[28] E. Schöll and P. T. Landsberg, Z. Phys. B **72**, 515 (1988).
[29] J. Kastrup, H. T. Grahn, K. Ploog, F. Prengel, A. Wacker, and E. Schöll, Appl. Phys. Lett. **65**, 1808 (1994).
[30] G. Schwarz, M. Patra, F. Prengel, and E. Schöll, Superlattices Microstruct. (to be published).
[31] P. Drazin, *Nonlinear Systems, Cambridge Texts in Applied Mathematics 10* (Cambridge University Press, Cambridge, 1992).
[32] J. Guckenheimer and P. Holmes, *Nonlinear Oscillations, Dynamical Systems, and Bifurcations of Vector Fields, Applied Mathematical Sciences 42* (Springer-Verlag, Berlin, 1983).
[33] Y. Zhang, R. Klann, K. H. Ploog, and H. T. Grahn, Appl. Phys. Lett. **70**, 2825 (1997).